Electrochemistry Communications 114 (2020) 106705

Contents lists available at ScienceDirect

Electrochemistry Communications

journal homepage: www.elsevier.com/locate/elecom

# Impact of lithium-ion coordination in carbonate-based electrolyte on lithium-ion intercalation kinetics into graphite electrode

Satoshi Uchida[a,*], Tomohide Katada[b], Masashi Ishikawa[b]

[a] Department of Energy and Environment, National Institute of Advanced Industrial Science and Technology, 1-8-31 midorigaoka, Ikeda, Japan
[b] Department of Chemistry and Materials Engineering, Faculty of Chemistry, Materials and Bioengineering, Kansai University, 3-3-35 yamate-cho, Suita, Japan

ARTICLE INFO

*Keywords:*
Lithium-ion intercalation kinetics
Desolvation process
Coordination state
Graphite electrode/electrolyte interface

ABSTRACT

The present paper provides a new perspective regarding the influence of anions on the rate of lithium ion insertion into graphite. We compared the properties of a LiFSA and solvent system with those of $LiPF_6$ system containing the same solvent when the ionic conductivity of these systems is comparable, to elucidate that better rate properties of the former system than the latter is well reflected in the lower desolvation resistance ($R_{desolv}$) and its lower activation energy ($E_a^{desolv}$) of the former. The solvation circumstances around $Li^+$ are similar for both the LiFSA and $LiPF_6$ systems, while a significant interaction between $Li^+$ and an anion is observed only in the former. In addition to the previously proposed hypothesis that the $E_a^{desolv}$ reflects the energy required to desolvate $Li^+$ from the last solvating molecule, the present result points to the necessity of considering the influence of the counter anion.

## 1. Introduction

Replacing the current fossil fuel-based automobiles by electric vehicles (EVs) powered by lithium-ion batteries (LIBs) is considered a way to mitigate the environmental burden caused by the $CO_2$ emission. A challenge to make EVs competitive is to shorten their full-charging time to 5–10 min, *i.e.*, time required to fill the fuel tank of the conventional gas vehicles, which translates into a significantly high rate of 6–12C. The input performance of LIBs strongly depends on the electrolyte [1,2], hence its further development is called for.

Our previous study has demonstrated that the rate performance of the LIBs could be significantly improved when we used an electrolyte solution consisting of lithium bis(fluorosulfonyl)amide (LiFSA) dissolved in a binary solvent of ethylene carbonate (EC) and dimethyl carbonate (DMC) of which the volumetric ratio is 10:90 [3]. In the course of developing this electrolyte system, we found that the combination of low EC-content solvent and LiFSA is a key to the superior kinetics. The present study intends to shed light on the origins of the superior kinetics. The dominant process governing the charging rate of current LIBs is the $Li^+$ intercalation into graphite, the mainstream negative electrode, the kinetics of which is influenced by three factors; namely, the ionic conductivity of the electrolyte [4], the desolvation of $Li^+$ from the electrolyte[5–7] and the ion diffusion in the solid electrolyte interface (SEI) film [13,14]. In the present study, by comparing four electrolyte systems containing LiFSA and $LiPF_6$ with different EC contents, we investigate how the intercalation kinetics is related to the electrolyte conductivity and the Raman spectra of not only the solvent in the solution but also the counter anion; the effect of the latter has been often considered insignificant in discussing the rate properties of LIBs.

## 2. Experimental

All the solvent and lithium salt (*i.e.*, $LiPF_6$, LiFSA, EC, DMC and GBL) of the lithium battery grade were purchased from Kishida Chemical. The electrolyte solutions were prepared in an argon-filled glove box with the dew point of below −70 °C to avoid reactions with moisture. EC and DMC were mixed with a volumetric ratio of 50:50 or 10:90. $LiPF_6$ or LiFSA salt was dissolved in these binary solvents to 1 mol $dm^{-3}$. In this paper, these electrolytes are labeled as (anion species)-(EC content); *e.g.*, $PF_6$-EC50, FSA-EC10, *etc*. We also use the terminology like “EC50 solvent” or “FSA systems” to abbreviate the expressions “solvent composed of 50 vol% of EC and 50 vol% of DMC” or “electrolyte systems containing LiFSA”. For Raman spectroscopy of the FSA system, the electrolytes in which EC is replaced by gamma-butyrolactone (GBL) were also prepared, which are labeled as FSA-GBL50 and FSA-GBL10.

The ionic conductivity of the electrolytes was measured by the electrochemical impedance technique using potentiogalvanostat (Ivium, CompactStat.e) equipped with a frequency response analyzer

* Corresponding author.
*E-mail address:* satoshi-uchida@aist.go.jp (S. Uchida).

https://doi.org/10.1016/j.elecom.2020.106705
Received 6 January 2020; Received in revised form 2 March 2020; Accepted 2 March 2020
Available online 06 March 2020

and a four-electrode cell (EC frontier). The cell constant was calibrated by using a KCl conductivity standard solution. The cell containing about 10 ml of each electrolyte, which was assembled and sealed air-tight in the glove box, was immersed in a water bath of which the temperature was controlled by a heater and coolant water within an accuracy of ± 0.1 °C. Alternative current (AC) impedance was measured at 15, 25, 35, 45, and 55 °C. The cell was equilibrated at each temperature for 20 min prior to the measurement. The AC frequency ranges from 200 to 10 kHz with the amplitude of 5 $mV_{p-0}$. The ionic conductivity was calculated from reciprocal of the real component of the obtained impedance and the cell constant.

Graphite (10 μm), acetylene black (Denka, Li-400), sodium carboxymethyl cellulose (DKS, WSA), and styrene-butadiene rubber (JSR, TRD2001) were homogeneously dispersed in deionized water with a weight ratio of 95:3:1:1 and the obtained slurry was cast on a Cu-foil current collector. After drying under vacuum and pressing, the electrode sheet was cut into 12-mm diameter disks for the electrochemical measurements. The mass loading of active material and its density are about 5.0 mg $cm^{-2}$ and 1.35 g $cm^{-3}$, respectively. The graphite electrode half-cells were assembled in the glove box with a lithium foil (Honjo Metal) of 13-mm diameter disk as the counter electrode, a highly porous polyolefin film coated with ceramic as the separator and the aforementioned electrolytes.

The $Li^+$ intercalation kinetics into the graphite electrode in each electrolyte was evaluated by potential step chronoamperometry and electrochemical impedance measurement. In this paper, we refer to the lithiation process (*i.e.*, the direction in which the cell voltage decreases) as "charge" and the reverse process as "discharge". Prior to the chronoamperometry, the graphite half-cells were pre-cycled so as to sufficiently form the solid/electrolyte interface on the graphite surface through the following procedure. Initially, the cells were charged to 5 mV with a constant current (C.C) mode followed by a constant voltage (C.V) mode, in the latter of which the current was cut off when it decreased to a tenth of the C.C mode, and discharged to 1500 mV with a C.C mode at 0.1 C-rate. Subsequently, the cells were cycled 10 times with the same voltage range and mode at 1 C-rate. After the pre-cycles, the cells were C.C-charged to 220 mV at 1C-rate and then held at that voltage for 1 h. For the chronoamperometry, the cell voltage was stepped down from 220 mV to 170 mV and the current response was recorded as a function of time by using a potentiogalvanostat (Solartron analytical, 1470E). The pre-cycles and the chronoamperometry were carried out at 25 °C. For the electrochemical impedance measurement, a graphite electrode symmetric cell was assembled as follows in order to eliminate the influence from the counter electrode. At first, two graphite half-cells, which consist of the electrodes with an equal active material mass, were pre-cycled under the same conditions as in the chronoamperometry, and then the cells were charged to 75% state of charge. After relaxing the cells at the open circuit voltage for 6 h, the two graphite electrodes were taken out from the cells in the glove box to re-assemble in a symmetric cell. The AC impedance was measured at 5, 10, 15, 20, and 25 °C using a multi electrochemical measurement system (Hokuto denko, HZ-Pro). The cell was held at each temperature for 50 min prior to the measurement. The AC frequency ranges from 500 kHz to 10 mHz with the amplitude of 5 $mV_{p-0}$.

Raman spectra of the electrolyte solutions were measured at room temperature to investigate the coordination state around $Li^+$ by using a laser Raman microscope (nano photon, RAMANtouch VIS-NIR-LT). The solutions were filled in a quartz cell with the 1 × 1-$cm^2$ cross section in the glove box. The exposure time was 1 s and the scattering spectrum was integrated 60 times. The wavenumber of the Raman shift was calibrated by the spectrum of a Si wafer standard.

## 3. Results and discussion

Fig. 1 indicates the Arrhenius plots of the conductivity $\sigma$ of the four electrolyte systems: $PF_6$-EC50, $PF_6$-EC10, FSA-EC50 and FSA-EC10. The

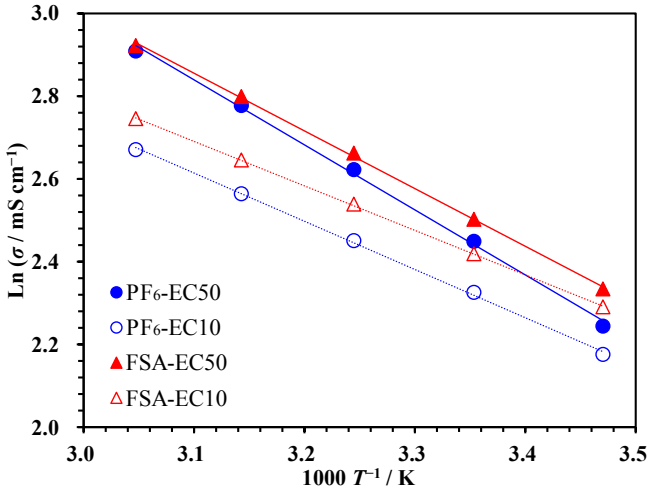


**Fig. 1.** Logarithm of the specific conductivity, ln $\sigma$, of the four electrolytes vs. the reciprocal temperature $1/T$, of which the slope gives $-E_a^{\sigma}/R$, measured by AC impedance spectroscopy in a four-electrode cell. Numerical data are available in Table S1.

numerical data are available in Table S1, which also summarizes the activation energy $E_a^{\sigma}$ derived from the equation $\ln \sigma = -E_a^{\sigma}/RT + C$ where $R$ is the gas constant, $T$ is the absolute temperature and $C$ is a constant. In the solvent EC50, $\sigma$ of the solute with FSA only slightly exceeds that with $PF_6$ (at most by 10% at 25 °C) throughout the temperature range in the present study, which is reflected in their comparable $E_a^{\sigma}$ in Table S1. When the EC content decreases from EC50 to EC10, regardless of the FSA- or $PF_6$-anion system, both $\sigma$ and $E_a^{\sigma}$ significantly decrease, resulting in a comparable $\sigma$ for all systems at room temperature. One might hence infer that neither the solvent composition (EC50 or EC10) nor the counter anion ($PF_6$ or FSA) is relevant in determining the reaction rate of the graphite electrode at room temperature, which is not the case in the present study as shown and proved below.

Fig. 2 shows the chronoamperogram of the graphite half-cells of the four electrolytes. We consider that the observed current only reflects the electrochemical behavior of the graphite electrode because the reaction rate of the counter electrode (*i.e.*, the dissolution of lithium metal) far exceeds that of the working electrode. The initial high current decaying within a few seconds stems from the double-layer

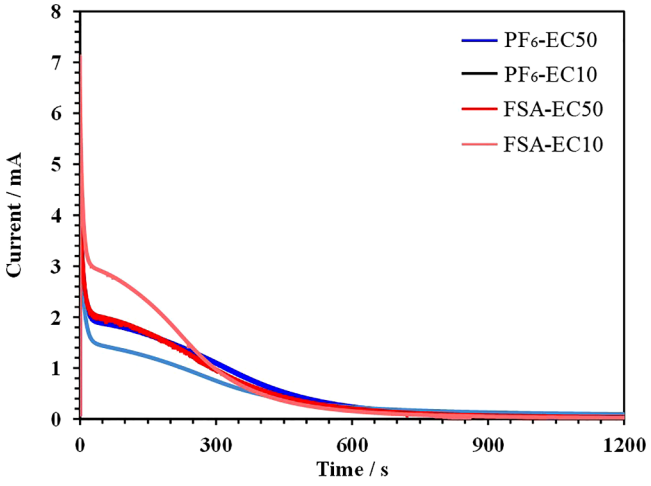


**Fig. 2.** Chronoamperogram of the graphite half-cells at 25 °C using the four electrolytes. Response to the cell voltage stepdown from 220 to 170 mV, prior to which the cell voltage was held at 220 mV for 1 h after 11 cycles of full charge and discharge.

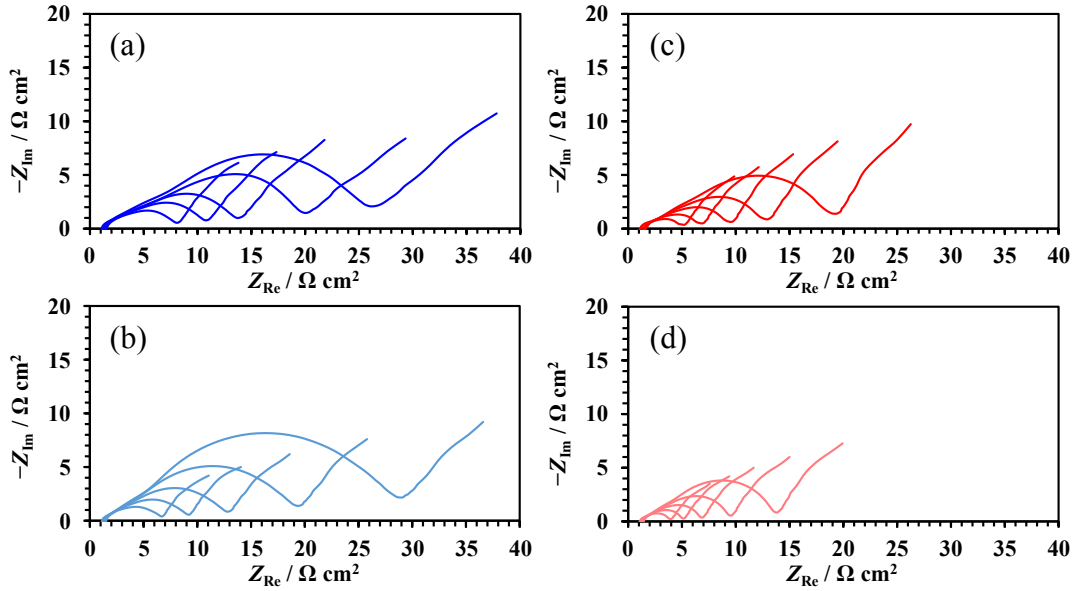


**Fig. 3.** Nyquist plot obtained from the AC impedance measurement of symmetric-cells with twin graphite electrodes (frequency: 500 kHz–10 mHz, amplitude: 5 $mV_{p-o}$, temperature: every 5 °C from 5 to 25 °C). (a) $PF_6$-EC50 (b) $PF_6$-EC10, (c) FSA-EC50 and (d) FSA-EC10. Before assembling the symmetric cells, each single electrode was cycled under the same conditions of the chronoamperometry and charged to 75% of the state of charge in the half-cell setup.

charging [8], which is irrelevant in determining the charging rate of the LIBs. The subsequent slow process corresponds to the $Li^+$ intercalation. In the solvent EC50, the intercalation current profiles are nearly the same for the $PF_6$ and FSA system. On the other hand, despite the comparable conductivity for all the four systems, not only is the profile significantly influenced by the decrease in the EC content from EC50 to EC10, but also current trend in decreasing EC for the $PF_6$ and FSA systems is opposite. Namely, the initial intercalation current of FSA-EC10 is approximately 1.5 times higher than that of FSA-EC50, while $PF_6$-EC10 shows smaller initial current than $PF_6$-EC50. The high initial current of FSA-EC10 results in a quicker charging than FSA-EC50 as indicated in the faster decay of the former current which falls below the latter after 300 s. That is, for the LiFSA system, reducing the EC content enhances the $Li^+$ intercalation kinetics. On the other hand, the rate of $PF_6$-EC10 is obviously slower than that of $PF_6$-EC50. Surely the ionic conductivity of the electrolyte can be an important factor to determine the rate performance of the LIBs. Yet even if the conductivity is comparable, the reaction kinetics varies with the solvent composition and/or the counter-anion.

Fig. 3 shows the Nyquist plots obtained from the AC impedance measurement of the graphite electrode symmetric cells. The high frequency limit, which corresponds to the bulk electrolyte resistance $R_s$, intercepts the $Z_{RE}$-axis at a similar point for all the cells. This reflects the fact that the conductivity of all the electrolytes in the present study is close to each other at room temperature. The multi-semicircular feature of the impedance in the high and intermediate frequency range, which overwhelms $R_s$ in magnitude, depends significantly on the temperature as well as on the electrolyte composition. When the EC content decreases from 50% to 10%, the semicircles shrink (except for the $PF_6$ system at 5 °C), which is, so long as the FSA system is concerned, consistent with the increased current observed in the chronoamperometry (Fig. 2), yet at odds for the $PF_6$ system where the current decreases. We analyzed the Nyquist plots based on the equivalent circuit shown in Fig. 4(a). As we failed to split the multi-semicircle into two components, we decided to do with three components, which can be interpreted as the electronic resistance $R_e$, the resistance of solid electrolyte interface $R_{SEI}$, and the resistance associated with the desolvation of $Li^+$ from electrolyte $R_{desolv}$ [6] which is often conventionally described as charge transfer resistance, respectively, in the descending order of frequency, where the crucial index in determining the input performance of the LIBs are the $R_{SEI}$ and $R_{desolv}$ characterizing the intermediate frequency regime because they are highly possible to dictate the kinetics of $Li^+$ intercalation into graphite [9,10]. Fig. S1 graphically illustrates an example of breaking down the Nyquist plot into the components in Fig. 4(a). The activation energy associated with the ion diffusion in SEI film $E_a^{SEI}$ and the desolvation process $E_a^{desolv}$ are evaluated from the slope of the Arrhenius plot, $\ln(1/R) = -E_a/RT + C$, shown in Fig. 4 (b and c). The results are summarized in Table S2 and S3**.** The trend in the magnitude of $R_{desolv}$ and $R_{SEI}$ as well as $E_a^{SEI}$ has no clear correlation with Fig. 2, where the current increases for the FSA system while decreases for the $PF_6$ system when the EC content decreases. The observation implies that these resistances strongly depends on the SEI in which the anions and solvents should be intricately involved. On the other hand, $E_a^{desolv}$ observed in this study well correlates with the current observed in Fig. 2. That is, in the EC50 electrolytes, either for the $PF_6$ or FSA system, $E_a^{desolv}$ is *ca.* 50 kJ $mol^{-1}$, which agrees with the previous study [6]. In the EC10 electrolytes, $E_a^{desolv}$ increases to 70 kJ $mol^{-1}$ or higher in the $PF_6$ system whereas it decreases to 40 kJ $mol^{-1}$ or lower in the FSA system. The present results can corroborate the consideration by Abe et al. that the desolvation process determines the reaction rate of the graphite electrode [6] except for the diffusion-limited cases, which can occur when the higher load electrode is used [11,12]. Incidentally, there is a debate that separating $R_{desolv}$ and $R_{SEI}$ in this way is problematic [13,14], about which we briefly addressed in the supporting information.

Fig. 5 compares the Raman spectra of (a) $PF_6$-EC50 and $PF_6$-EC10 and (b) FSA-EC50 and FSA-EC10. The signals from the solvent without salt are in Fig. S2. The peaks located around 892 and 915 $cm^{-1}$ are assigned to stretching vibration of C—O bond in free EC and free DMC, respectively [15,16]. The spectra obtained from $PF_6$ system look as similar to the FSA one, that is, they are not affected by the anions. It can be, therefore, interpreted that the peak shift is affected only by the interaction between the solvents and $Li^+$. These peaks shift to 904 and 932 $cm^{-1}$, when they solvate $Li^+$ [16]. The fraction *f* and the number *n* of molecules solvating $Li^+$ are summarized in Table 1, which were estimated from the peak area ratios and the molar ratio of the salt to the solvent in Table S4 [17] by assuming the invariance in the scattering cross section between free and solvating molecules. The results of peak separation using the asymmetric pseudo-Voigt function (Eq. S1) are shown in Fig. S3. Table 1 suggests that the solvation number *n* hardly

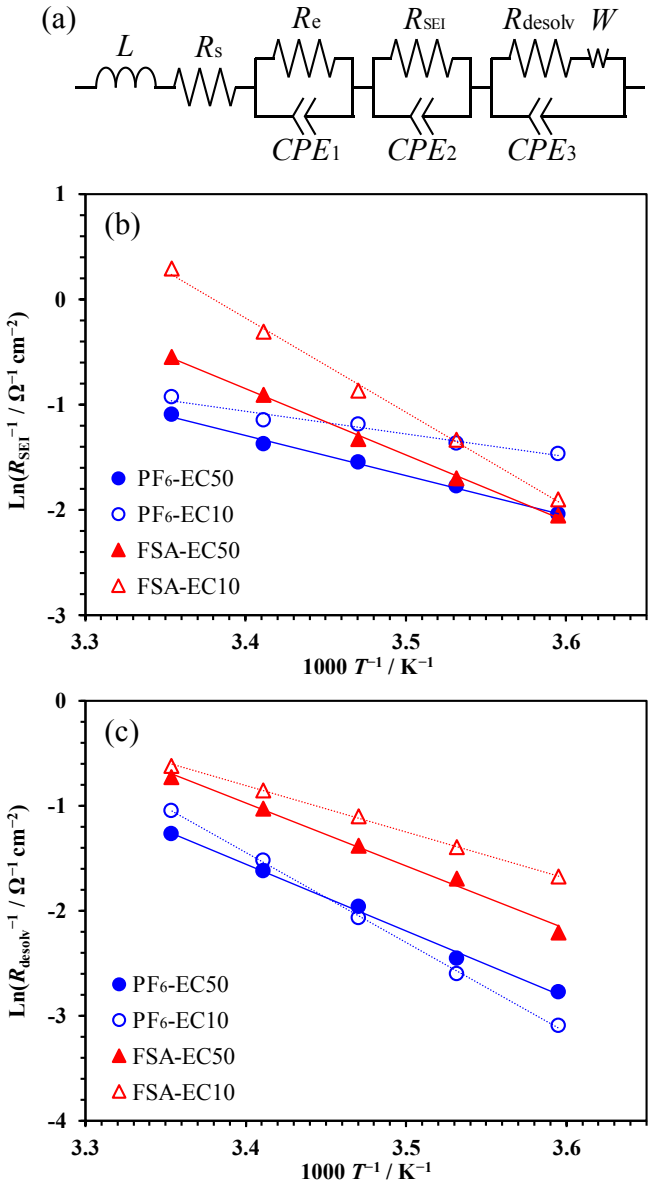


**Fig. 4.** (a) Equivalent circuit to model the impedance spectra in Fig. 3. *L*: inductance of the measurement cables; $R_s$, $R_e$, $R_{SEI}$ and $R_{desolv}$: resistance associated with the electrolyte bulk, electronic conduction in the electrode, ion diffusion in solid electrolyte interface (SEI) and desolvation of $Li^+$ from electrolyte, respectively; *W*: Warburg impedance of the ionic diffusion in graphite particle; $CPE_{1-3}$: constant phase element characterizing the non-uniform distribution of capacitance associated with the electron conduction, SEI and the desolvation, respectively. (b and c) Logarithm of the resistance of SEI film ln $1/R_{SEI}$ and the desolvation resistance ln $1/R_{desolv}$ vs. $1/T$ of which the slope gives $-E_a^{desolv}/R$ and $-E_a^{SEI}/R$, respectively.

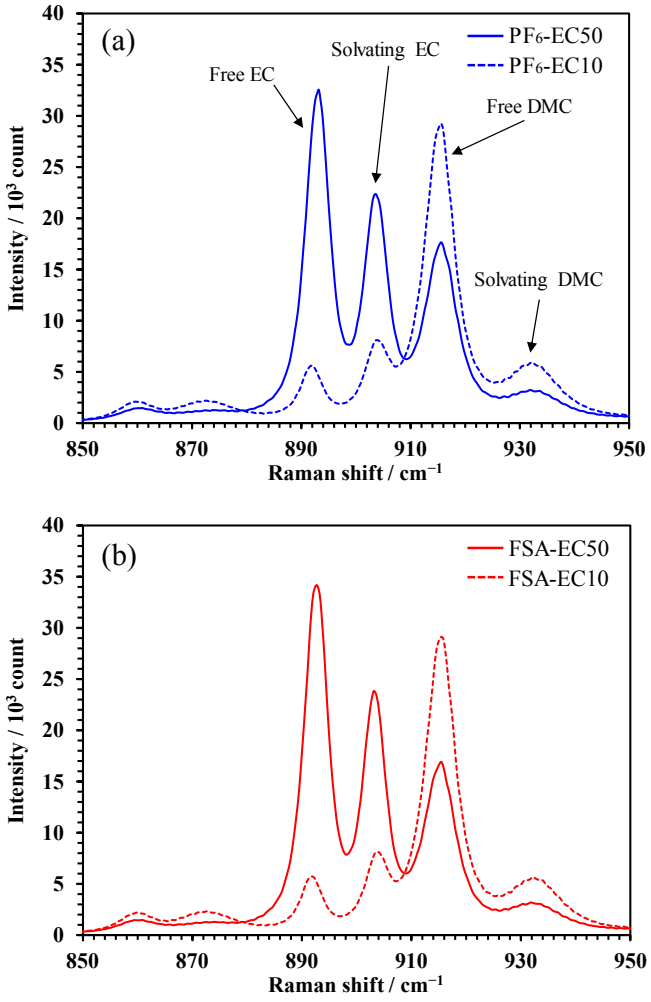


**Fig. 5.** Raman spectra at room temperature of (a) $PF_6$-EC50 and $PF_6$-EC10 and (b) FSA-EC50 and FSA-EC10. The peaks of which the top is located at (892, 904) and (915, 932) in $cm^{-1}$ derive from the stretching vibration of C–O bond in (free EC, solvating EC) and (free DMC, solvating DMC), respectively.

**Table 1**
Fraction *f* and the number *n* of solvent molecules solvating $Li^+$ estimated by analyzing the peak area in Fig. 5 using an asymmetric pseudo-Voigt function (see Eq. S1).

| Electrolyte | *f*/– | | *n*/– | | |
|---|---|---|---|---|---|
| | EC | DMC | EC | DMC | EC + DMC |
| $PF_6$-EC50 | 0.36 | 0.22 | 2.6 | 1.2 | 3.8 |
| $PF_6$-EC10 | 0.65 | 0.23 | 1.0 | 2.3 | 3.3 |
| FSA-EC50 | 0.35 | 0.22 | 2.5 | 1.2 | 3.7 |
| FSA-EC10 | 0.64 | 0.23 | 0.9 | 2.2 | 3.1 |

distinguishes the FSA-system from the $PF_6$-system. That is, either for the $PF_6$- or FSA-system, in the solvent EC50, about 2.5 EC molecules and slightly more than one DMC molecules solvate $Li^+$, totaling slightly less than four in $n_{total}$. When the EC content decreases to EC10, barely one EC molecule solvates $Li^+$ compensated partially by the increase in the number of DMC molecule to slightly more than two, resulting in the decrease in $n_{total}$ to nearly three. Yamada *et al.* hypothesize that $E_a^{CT}$ should reflect the energy associated with the step in which the last molecule leaves $Li^+$ in the sequential desolvation process during the intercalation into graphite [18]. By considering the stronger interaction of EC with $Li^+$ than DMC [19], this hypothesis should lead to the equal $E_a^{CT}$ since in all the four electrolyte systems $Li^+$ is solvated by at least one EC molecule. The present observation that $E_a^{CT}$ increases in the $PF_6$-system while it decreases in the FSA-system upon the decrease in the EC-content in the solvent implies that we have to take into account the influence from the counter anion.

The symmetric stretching vibration of $PF_6^-$ octahedron ($a_{1g}$ mode) shows up at 741 $cm^{-1}$ [20,21], which is hardly influenced by the EC-content as shown in Fig. 6(a), where the other peaks at 716 and 728 $cm^{-1}$ are assigned to the symmetric ring deformation of free and solvating EC [15,22]. The spectra of the salt-free solvent in this region can also be identified in Fig. S2. By considering the significant influence of the EC-content on the solvating circumstances around $Li^+$ described in the previous section, the invariance of the signal from $PF_6^-$ implies

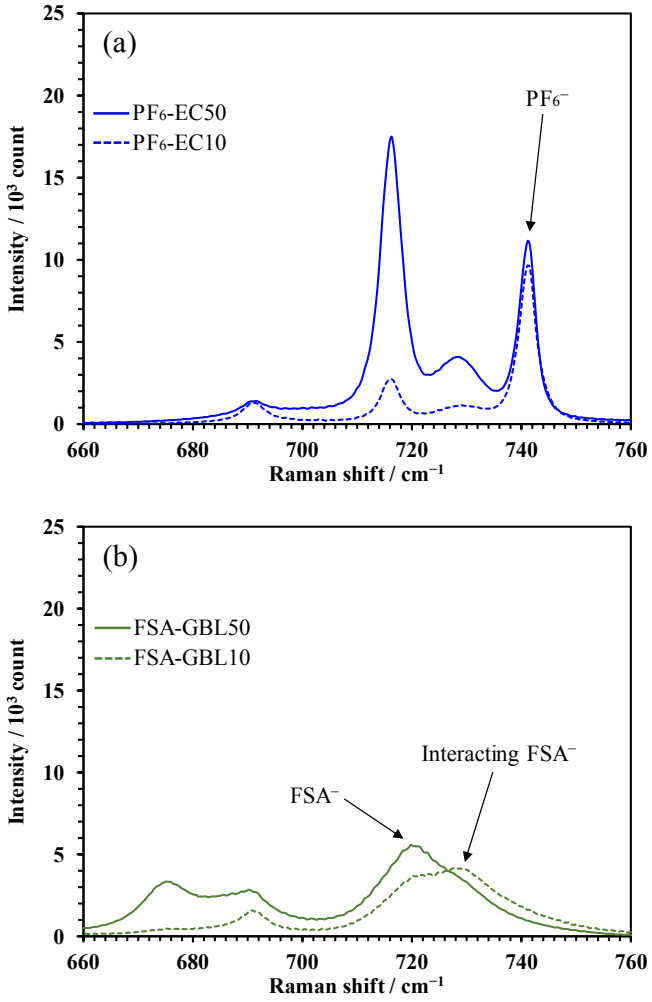


**Fig. 6.** Raman spectra at room temperature of (a) $PF_6$-EC50 and $PF_6$-EC10 where the peaks at 716 and 728 $cm^{-1}$ are assigned to the symmetric ring deformation of free and solvating EC, respectively, and at 741 $cm^{-1}$ derives from the symmetric stretching vibration of $PF_6^-$ ($a_{1g}$) and (b) FSA-GBL50 and FSA-GBL10 where the peaks at 720 and 729 $cm^{-1}$ relate to $FSA^-$.

that the cation-anion interaction is insignificant in the $PF_6$-systems. Because the relatively weak signal from $FSA^-$ is eclipsed by an intensive one from EC (Fig. S4), we replaced EC by GBL, of which the chemical structure and the dielectric constant are close to EC, so that we assume the effect of the solvent content on the ionic interactions can be qualitatively discussed. Fig. 6 (b) shows the Raman spectra of FSA-GBL50 and FSA-GBL10, where two peaks related to $FSA^-$ show up at $\nu_L$ = 720 and $\nu_H$ = 729 $cm^{-1}$. Although the assignment and interpretation of these signals differ by Refs. [23,24], one can say that $\nu_H$ should derive from $FSA^-$ more strongly interacting with $Li^+$ than $\nu_L$. When the GBL-content decreases from 50% to 10%, the fraction of $FSA^-$ that gives $\nu_H$ increases from 0.38 to 0.85, calculated from the peak area ratio of $\nu_H$ and $\nu_L$ (see Fig. S5). A similar qualitative tendency can apply for EC. The fact that $n_{total} > 3$ for all the systems suggests that there seems to be no room for the anion to come to the primary solvation shell of $Li^+$. Nonetheless, in the FSA-system, $FSA^-$ interacts with $Li^+$ probably from the secondary shell, where the $FSA^-$ influence is not reflected in the static solvation number.

The present study examined the kinetics of $Li^+$ intercalation into graphite from the viewpoint of the coordination state of the solvent and anion. However, an important role should also be played in determining the kinetics by the solid electrolyte interface (SEI), of which the investigation is admittedly insufficient; *e.g.*, how $R_{desolv}$ is related to $R_{SEI}$ [13,14], how the EC content influences the SEI composition [25–28] and so on. These issues are briefly addressed in the support information along with the XPS spectra reflecting the SEI composition (Figs. S6 and S7) and the temperature dependence of $1/R_{SEI}$ (Fig. S8).

## 4. Conclusions

The present study investigated the reason why the low EC-content electrolyte, 1 mol $dm^{-3}$ LiFSA in EC:DMC = 10:90 (by vol.), excels in the input performance for the graphite electrode. We compared the properties of the LiFSA system with $LiPF_6$ system dissolved in the same solvent, the ionic conductivity of which is comparable, to find that the higher rate properties of the former system than the latter is well reflected in the lower desovation resistance ($R_{desolv}$) and its lower activation energy ($E_a^{desolv}$) of the LiFSA system. That is, the rate of $Li^+$-intercalation into graphite is dominated by the process at the interface between graphite and the electrolyte, rather than the bulk electrolyte conductivity as long as the relativity low active material loading (~5 mg $cm^{-2}$, ~2 mAh $cm^{-2}$), although the rate performances would be more dominantly influenced by the bulk solution properties if a higher load electrode (*e.g.*, ~8 mAh $cm^{-2}$) is used. The Raman spectroscopy revealed that, from the viewpoint of solvation number, the circumstances around $Li^+$ are similar for either the LiFSA or $LiPF_6$ system, in which at least one EC molecule solvates $Li^+$. In addition to the hypothesis that $E_a^{desolv}$ reflects the energy required to desolvate $Li^+$ from the last solvating molecule, the present result points to the necessity of considering the influence from the counter anion; the Raman signal in the presence of $FSA^-$ clearly changes with the solvent composition while that in the presence of $PF_6^-$ does not. To further improve the rate properties of the electrolyte, detailed understanding of the many-body correlations of not only the cation and solvent but also the anion is important.

## Funding

This research did not receive any specific grant from funding agencies in the public, commercial, or not-for-profit sectors.

## CRediT authorship contribution statement

**Satoshi Uchida:** Conceptualization, Methodology, Investigation, Validation, Writing - original draft, Visualization. **Tomohide Katada:** Investigation. **Masashi Ishikawa:** Resources, Writing - review & editing.

## Declaration of Competing Interest

The authors declare that they have no known competing financial interests or personal relationships that could have appeared to influence the work reported in this paper.

## Appendix A. Supplementary data

Supplementary data to this article can be found online at https://doi.org/10.1016/j.elecom.2020.106705.

## References

[1] A. Guerfi, M. Dontigny, P. Charest, M. Petitclerc, M. Lagacé, A. Vijh, K. Zaghib, J. Power Sources 195 (2003) 845–852, https://doi.org/10.1016/j.jpowsour.2009.08.056.
[2] A. Lewandowski, A. Świderska-Mocek, J. Power Sources 194 (2009) 601–609, https://doi.org/10.1016/j.jpowsour.2009.06.089.
[3] S. Uchida, M. Ishikawa, J. Power Sources 359 (2017) 480–486, https://doi.org/10.1016/j.jpowsour.2017.05.090.
[4] T. Fukutsuka, K. Koyamada, S. Maruyama, K. Miyazaki, T. Abe, Electrochim. Acta 199 (2016) 380–387, https://doi.org/10.1016/j.electacta.2016.03.049.
[5] T. Abe, F. Sagane, M. Ohtsuka, Y. Iriyama, Z. Ogumi, J. Electrochem. Soc. 152

(2003) A2151–A2154, https://doi.org/10.1149/1.2042907.
[6] T. Abe, H. Fukuda, Y. Iriyama, Z. Ogumi, J. Electrochem. Soc. 151 (2004) A1120–A1123, https://doi.org/10.1149/1.1763141.
[7] T. Doi, T. Fukutsuka, K. Takeda, T. Abe, K. Miyazaki, Z. Ogumi, J. Phys. Chem. C 116 (2012) 12422–12425, https://doi.org/10.1021/jp302358v.
[8] M.D. Levi, E. Markevich, C. Wang, D. Aurbach, J. Electroanal. Chem. 600 (2007) 13–22, https://doi.org/10.1016/j.jelechem.2005.11.037.
[9] A. Funabiki, M. Inaba, Z. Ogumi, J. Power Sources 68 (1997) 227–231, https://doi.org/10.1016/S0378-7753(96)02556-6.
[10] A. Funabiki, M. Inaba, Z. Ogumi, S. Yuasa, J. Otsuji, A. Tasaka, J. Electrochem. Soc. 145 (1998) 172–178, https://doi.org/10.1149/1.1838231.
[11] H. Murayama, K. Kitada, K. Fukuda, A. Mitsui, K. Ohara, H. Arai, Y. Uchimoto, Z. Ogumi, E. Matsubara, J. Phys. Chem. C 118 (2014) 20750–20755, https://doi.org/10.1021/jp5029273.
[12] N. Ogihara, Y. Itou, T. Sasaki, Y. Takeuchi, J. Phys. Chem. C 119 (2015) 4612–4619, https://doi.org/10.1021/jp512564f.
[13] O. Borodin, G. Zhuang, P. Ross, K. Xu, J. Phys. Chem. C 117 (2013) 7433–7444, https://doi.org/10.1021/jp4000494.
[14] T. Jow, S. Delp, J. Allen, J. Jones, M. Smart, J. Electrochem. Soc. 165 (2018) A361–A367, https://doi.org/10.1149/2.1221802jes.
[15] G.J. Janz, J. Ambrose, J.W. Coutts, J.R. Downey Jr., Spectrochim. Acta 35A (1979) 175–179, https://doi.org/10.1016/0584-8539. (79)80181-6.
[16] D. Battisti, G.A. Nazri, B. Klassen, R. Aroca, J. Phys. Chem. 97 (1993) 5826–5830, https://doi.org/10.1021/j100124a007.
[17] M. Morita, Y. Asai, N. Yoshimoto, M. Ishikawa, J. Chem. Soc., Faraday Trans. 94 (1998) 3451–3456, https://doi.org/10.1039/A806278A.
[18] Y. Yamada, Y. Iriyama, T. Abe, Z. Ogumi, Langmuir 25 (2009) 12766–12770, https://doi.org/10.1021/la901829v.
[19] M. Okoshi, Y. Yamada, A. Yamada, H. Nakai, J. Electrochem. Soc. 160 (2013) A2160–A2165, https://doi.org/10.1149/2.074311jes.
[20] S.-D. Han, S.-H. Yun, O. Borodin, D.M. Seo, R.D. Sommer, V.G. Young Jr., W.A. Henderson, J. Phys. Chem. C 119 (2015) 8492–8500, https://doi.org/10.1021/acs.jpcc.5b00826.
[21] C.M. Burba, R. Frech, J. Phys. Chem. B 109 (2005) 15161–15164, https://doi.org/10.1021/jp058045f.
[22] B. Klassen, R. Aroca, M. Nazri, G.A. Nazri, J. Phys. Chem. B 102 (1998) 4795–4801, https://doi.org/10.1021/jp973099d.
[23] S.-D. Han, O. Borodin, D.M. Seo, Z.-B. Zhou, W.A. Henderson, J. Electrochem. Soc. 161 (2014) A2042–A2053, https://doi.org/10.1149/2.0101414jes.
[24] Y. Yamada, M. Yaegashi, T. Abe, A. Yamada, Chem. Commun. 49 (2013) 11194–11196, https://doi.org/10.1039/c3cc46665e.
[25] J. Alvarado, M. Schroeder, M. Zhang, O. Borodin, E. Gobrogge, M. Olguin, M. Ding, M. Gobet, S. Greenbaum, Y. Meng, K. Xu, Mater. Today 21 (2018) 341–353, https://doi.org/10.1016/j.mattod.2018.02.005.
[26] M. Nie, D. Abraham, D. Seo, Y. Chen, A. Bose, B. Lucht, J. Phys. Chem. C 117 (2013) 25381–25389, https://doi.org/10.1021/jp409765w.
[27] O. Borodin, M. Olguin, P. Ganesh, P. Kent, J. Allen, W. Henderson, Phys. Chem. Chem. Phys. 164 (2016) 164–175, https://doi.org/10.1039/c5cp05121e.
[28] O. Borodin, D. Smith, J. Phys. Chem. B 113 (2009) 1763–1776, https://doi.org/10.1021/jp809614h.